Electronic Supplementary Information

High specific surface area Fe-N-C electrocatalysts for oxygen reduction reaction synthesized by a hard-template-assisted ball milling strategy

Feng Sun,[a,b] Tao Liu,[b] Meihua Huang*[a,b] and Lunhui Guan*[a,b]

a. College of Chemistry, Fuzhou University, Fuzhou 350108, Fujian, P.R. China.

b. CAS Key Laboratory of Design and Assembly of Functional Nanostructures, and Fujian Provincial Key Laboratory of Nanomaterials, Fujian Institute of Research on the Structure of Matter, Chinese Academy of Sciences, Fuzhou, Fujian 350002, P.R. China

* Corresponding Author: meihuahuang@fjirsm.ac.cn ; guanlh@fjirsm.ac.cn

Experimental

1.1 Chemicals

Zinc oxide (ZnO, A.R. grade), Iron nitrate nonahydrate (Fe(NO$_3$)$_3$·9H$_2$O, A.R. grade), 2-methylimidazole (C$_4$H$_6$N$_2$, A.R. grade), sodium chloride(NaCl, A.R.grade), hydrochloric acid(HCl, A.R.grade) were bought from Shanghai Aladdin Biochemical Technology Co., Ltd. Perchloric acid (HClO$_4$) and Nafion solution (5.0 wt.%) were bought from Sigma-Aldrich. 2-Propanol ((CH$_3$)$_2$CHOH, 99+% grade) and Pt/C (20.0 wt.%) were bought from Alfa Aesar. All reagents are used directly without further treatment.

1.2 Synthesis of Fe-ZIF@NaCl

The Fe-ZIF@NaCl precursor was synthesized via method following the low energy ball milling method, which has been optimized accordingly. In detail, 0.57g ZnO, 1.15g 2-methylimidazole and 2.5g NaCl were mixed in a Nylon ball mill can (volume 50 mL). And 1 mL of t mmol/L (t=0, 0.07, 0.14, 0.21, 0.35) Iron nitrate nonahydrate aqueous solution

were added to the ball mill can, then the agate beads which accounted for 50% of the can's volume were added rapidly. The ball mill can was then placed in a planetary ball mill and run for 180 minutes at 200 revolutions per minute. The slurry product was washed with water for three times by vacuum filtration and dried at 80°C overnight. The dried precursor was ground in agate mortar and heated to 950°C for 2h with a heating rate of 3 °C min^{-1} under N$_2$ flow protection. The black powder was stirred in 1 mol/L of hydrochloric acid at 60°C for 15 hours, then washed and dried. The dried power was heated to 950°C for 2h with a heating rate of 3 °C min^{-1} under N$_2$ flow protection. Finally, the obtained powder was denoted as the x%Fe-ZIF@NaCl samples (x refers to the mole ratio of Fe: Zn). The 0Fe-ZIF@NaCl was prepared with not adding iron nitrate nonahydrate aqueous solution but 1 mL deionized water. The 2%Fe-ZIF was prepared as the same way of 2%Fe-ZIF@NaCl but without NaCl added. NC was prepared with not adding NaCl and Iron nitrate nonahydrate aqueous solution but 1 mL deionized water. The quantity of NaCl was changed from 1.5g to 6g, and the correspondent samples were denoted as the 2%Fe-ZIF@1.5NaCl, 2%Fe-ZIF@3NaCl, 2%Fe-ZIF@6NaCl.

1.3 Synthesis of ZIF-8 precursor

The ZIF-8 precursor was synthesized via method as follows. In detail, 0.57g ZnO, 1.15g 2-methylimidazole were mixed in a Nylon ball mill can (volume 50 mL). And 1 mL deionized water were added to the ball mill can, then the agate beads which accounted for 50% of the can's volume were added rapidly. The ball mill can was then placed in a planetary ball mill and run for t (t=10, 30, 60, 180, 720) minutes at 200 revolutions per minute. The slurry product was washed with water for three times by vacuum filtration and dried at 80°C overnight. Finally, the obtained powder was denoted as the ZIF-t. The ZIF-180@NaCl was prepared as the same way of ZIF-180 but with 2.5g NaCl added.

Characterization

Transmission electron microscopy (TEM) and high-resolution TEM (HR-TEM) images were obtained by using the Tecnai F20 microscope. X-ray diffraction (XRD) measurements were performed with a Miniflex600 diffractometer using a Cu Kα (λ =

1.5405 Å) radiation source. X-ray photoelectron spectroscopy (XPS) analysis was performed on an ESCALAB 250Xi X-ray photoelectron spectrometer (Thermo, America). N_2 isothermal adsorption/desorption was recorded by a Brunauer-Emmett-Teller surface area analyzer (BET, Quantachrome Autoscorb-iQ2-XR) at 77K. Fe content in the synthesized samples was obtained by Inductively Coupled Plasma Optical Emission Spectrometer (ICP-OES, Ultima-2), dissolved by aqua regia solution. The X-ray absorption fine structure spectra (Fe K-edge) were collected at BL11B station in Shanghai Synchrotron Radiation Facility (SSRF). The Fe K-edge spectra of all the samples were recorded under fluorescence excitation mode using a Lytle detector except for the Fe foil, which was measured with transmission mode. The XAS data were analyzed by the Athena and Artemis software. The nuclear magnetic resonance (NMR) was performed on JNM-ECZ600R/S1.

Electrochemistry measurement

All of the electrochemical measurements were performed on a CHI 760D electrochemical station (Shanghai Chenhua, China) equipped with a conventional three-electrode system. The reference electrode was an Ag/AgCl electrode (saturated KCl), the counter electrode was a graphite rod electrode and the working electrode was a glassy carbon rotating disk electrode (GC-RDE) with a diameter of 5.0 mm, and 0.1 M $HClO_4$ as the acidic electrolytes. All of the potentials reported in this work were calibrated to the reversible hydrogen electrode (RHE). Catalysts inks were prepared by dispersing 5 mg of catalyst in a solution of 960 μl isopropanol and 40 μl Nafion (5 wt%, Aldrich), and then applying sonication for 3 hours to form a uniform ink. The working electrode was prepared through a drop casting strategy. 30 μl of the ink was loaded onto the GC electrode with a catalyst loading of ~0.8 mg cm^{-2}. But for commercial Pt/C (20 wt%) catalyst, 4 μl of the ink was loaded onto the GC electrode with a catalyst loading of ~0.100 mg cm^{-2}. For the electrochemical ORR test, O_2 was first pumped into a 0.1 M $HClO_4$ aqueous solution for 30 minutes to reach oxygen saturation, and then a cyclic voltammeter (CV) scan was performed at 100 mV s^{-1} in the potential range of 0.056-1.056V until reaching a stable CV

diagram. Then we conducted LSV tests within the same potential ranges as the CV measurements, at the sweep speed of 10mV s^{-1} and the rotation speed of 1600rpm. LSV and CV curves were also recorded under N$_2$ conditions, used to deduct the background. The stability was examined by CV. The ADT in acid medium was conducted in O$_2$-saturated 0.1 M HClO$_4$ solution at a scan rate of 200 mV s^{-1} with the potential between 0.6 V and 1.0 V *vs.* RHE for 10000 cycles.

The kinetic current density (J$_K$) was calculated by Koutecky-Levich equation:

$$\frac{1}{j} = \frac{1}{j_K} + \frac{1}{j_L}$$

Where J$_L$ and J is diffusion limited current density at 0.4 V (VS. RHE) and the measured current density, respectively. Then, we plotted the J$_K$ and potential at Logarithmic scales. The straight lines near the half-wave potential were used for linear fitting.

Assemblies and tests of H$_2$-O$_2$ fuel cells

Cathode and anode catalyst inks were made by dispersing the catalyst in isopropanol to water (9:1) solvent mixture with Nafion (5 wt%) at an ionomer to catalysts ratio (I/C) of 0.8, and then sonicated for 30 mins. The catalyst-coated-membrane (CCM) with an area of 5 cm^2 was prepared by spraying ink on Nafion 211. The cathode catalyst load was 2 mg cm^{-2} and the anode catalyst (Pt/C, 40 wt%) load was 0.2 mg$_{pt}$ cm^{-2}. The fabricated CCM was dried to completely evaporate the solvents. Two gas diffusion layers (GDLs), two gaskets, and the prepared CCM were pressed to obtain the membrane electrode assembly (MEA). For H$_2$-O$_2$ single cell tests, 80% relative humidity and the cell temperature was maintained at 80 ℃. The backpressure was maintained at 1.5 bar, and the flow rates of H$_2$ and O$_2$ were 200 mL min^{-1} and 500 mL min^{-1} respectively (1 000 mL min^{-1} for air flow). Prior to the data collection, an MEA activation was applied for 3 hours and then polarization curves of fuel cell were recorded by stepping voltages starting at 0.90V and decreasing by 2mV per seconds until 0.3V by SMART2.
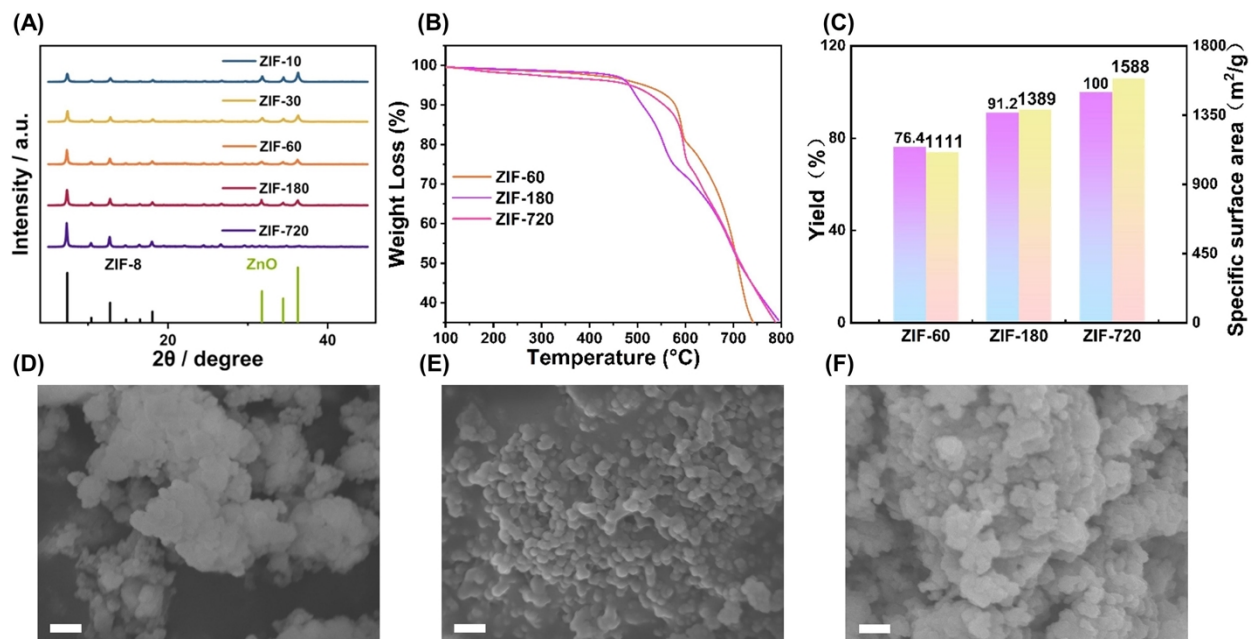
Fig. S1 (A) XRD patterns of ZIF-10, ZIF-30, ZIF-60, ZIF-180 and ZIF-720;(B) TGA curves of ZIF-60, ZIF-180 and ZIF-720;(C) Yield and specific surface area of ZIF-60, ZIF-180 and ZIF-720;(D) SEM image of ZIF-60; (E) SEM image of ZIF-180; (F) SEM image of ZIF-720. The measuring scale of (D)(E)(F) was 500nm.
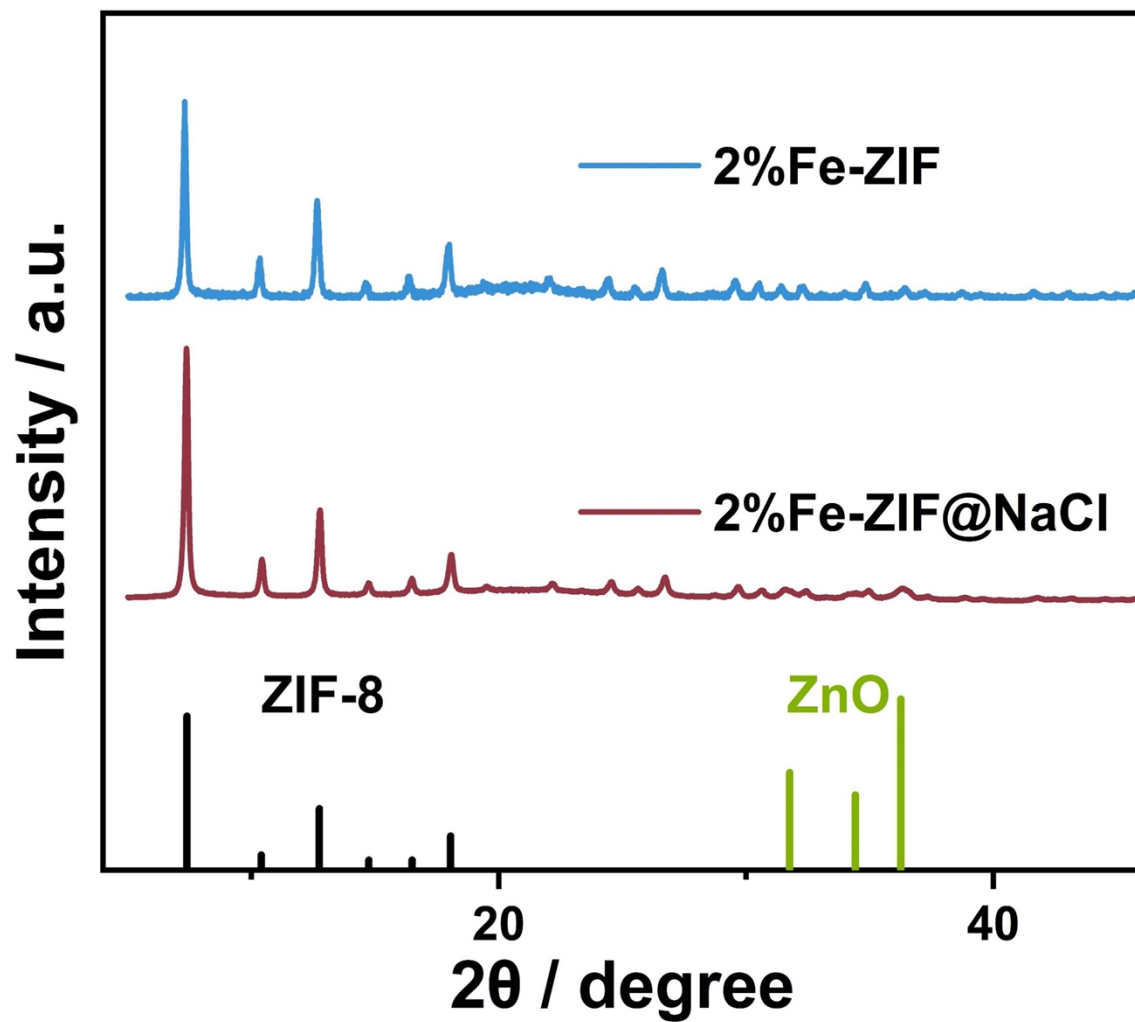
Fig. S2 XRD patterns of 2%Fe-ZIF@NaCl and 2%Fe-ZIF.
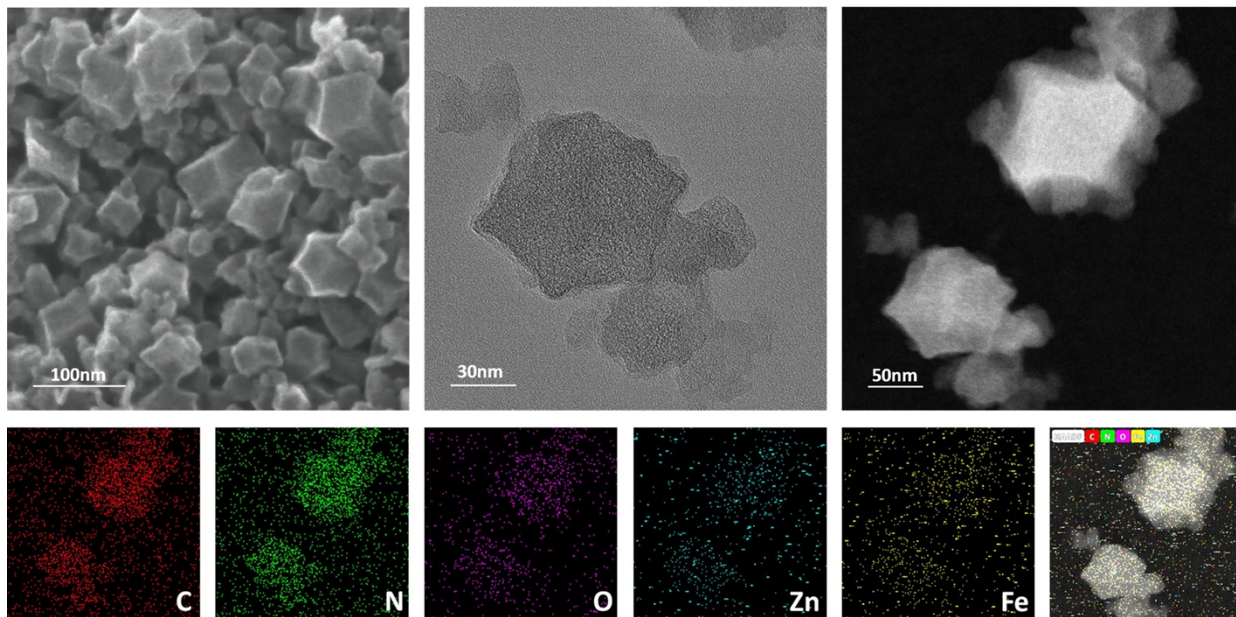
Fig. S3 (A) SEM image;(B) TEM image;(C) STEM image;(D–I) HAADF-STEM-EDS elemental mappings of 2%Fe-ZIF.
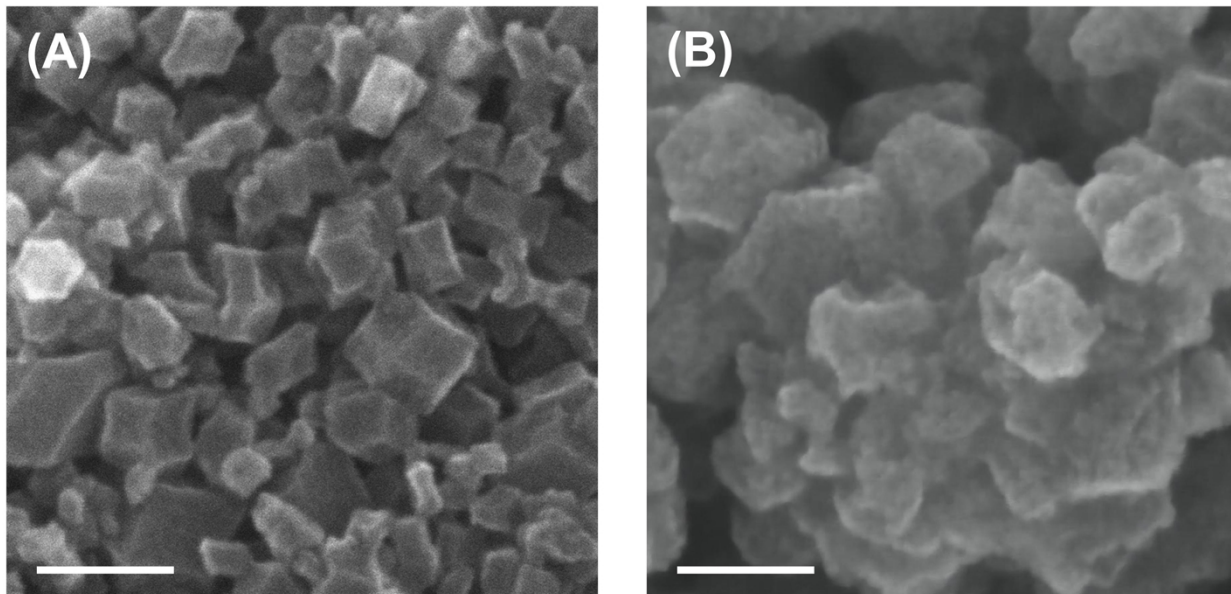
Fig. S4 (A) SEM image of pyrolyzed ZIF-180;(B) SEM image of pyrolyzed ZIF-180@NaCl. The measuring scale of (A)(B) was 100nm.
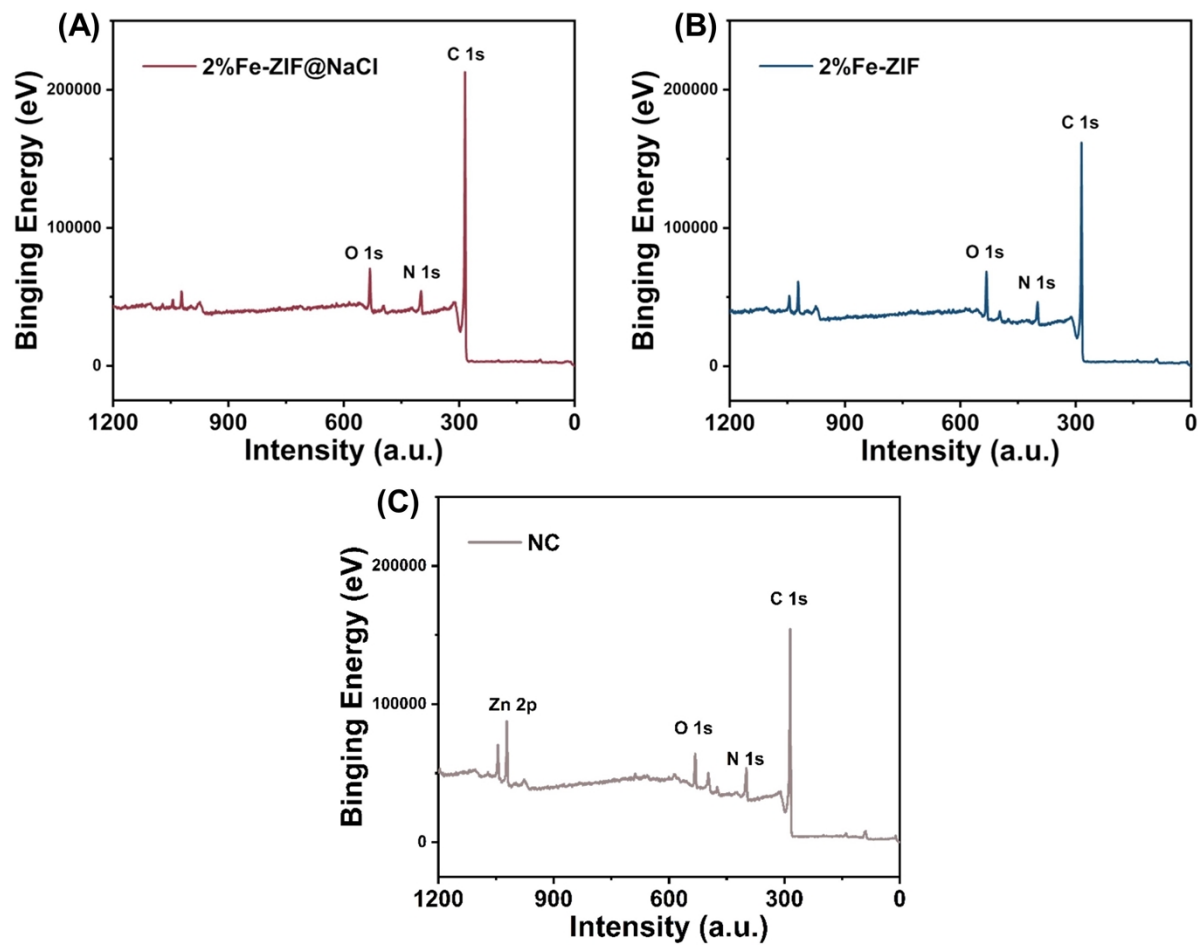
Fig. S5 XPS spectra of (A) 2%Fe-ZIF@NaCl, (B) 2%Fe-ZIF and ,(C)NC
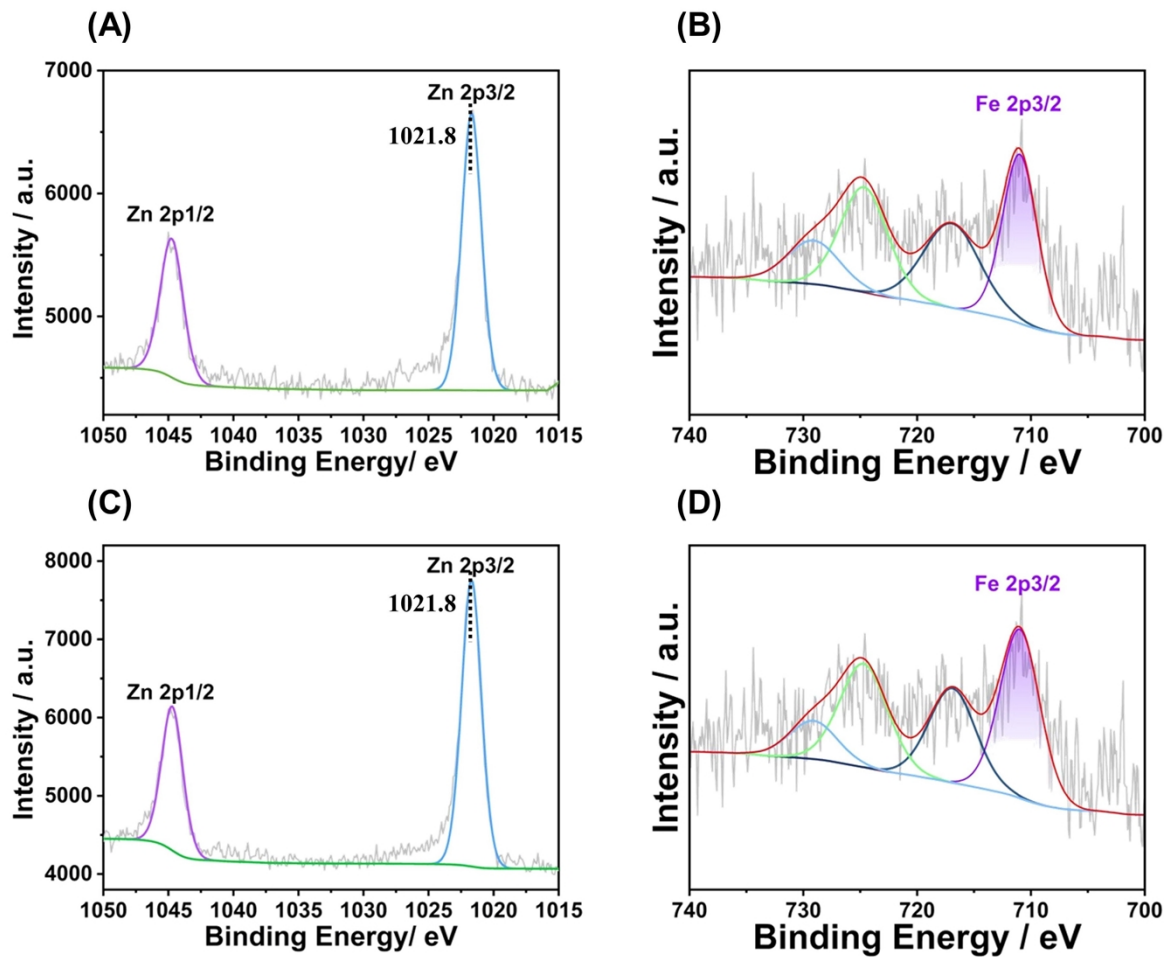
Fig. S6 (A) Zn 2p analysis and (B) Fe 2p analysis of 2%Fe-ZIF@NaCl; (C) Zn 2p analysis and (D) Fe 2p analysis of 2%Fe-ZIF.
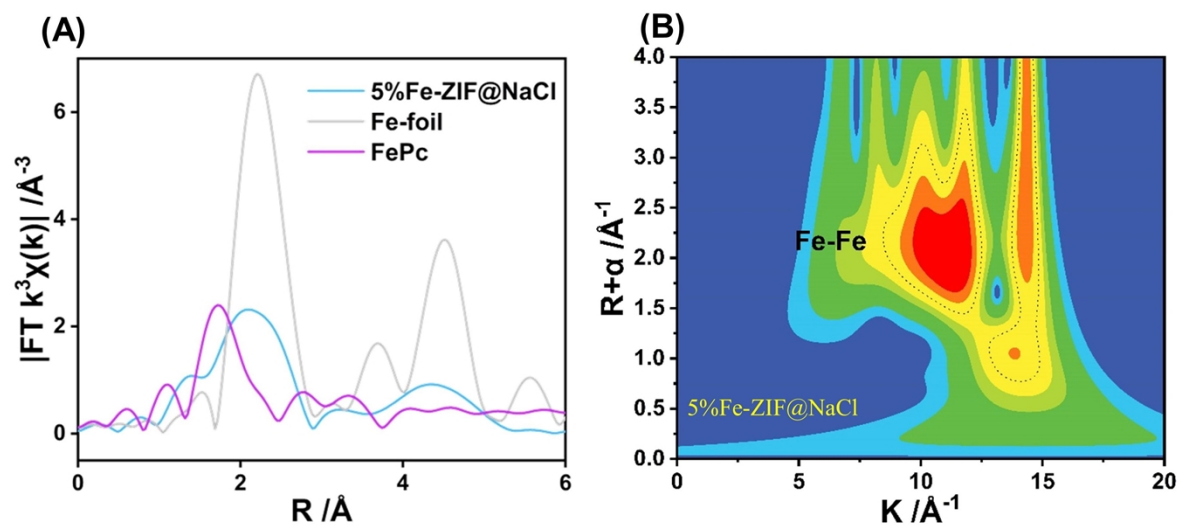
Fig. S7 (A) k3-weighted Fourier transforms of EXAFS spectra of 5%Fe-ZIF@NaCl, Fe-foil and FePc;(B) k3-weighted wavelet-transform of 5%Fe-ZIF@NaCl.
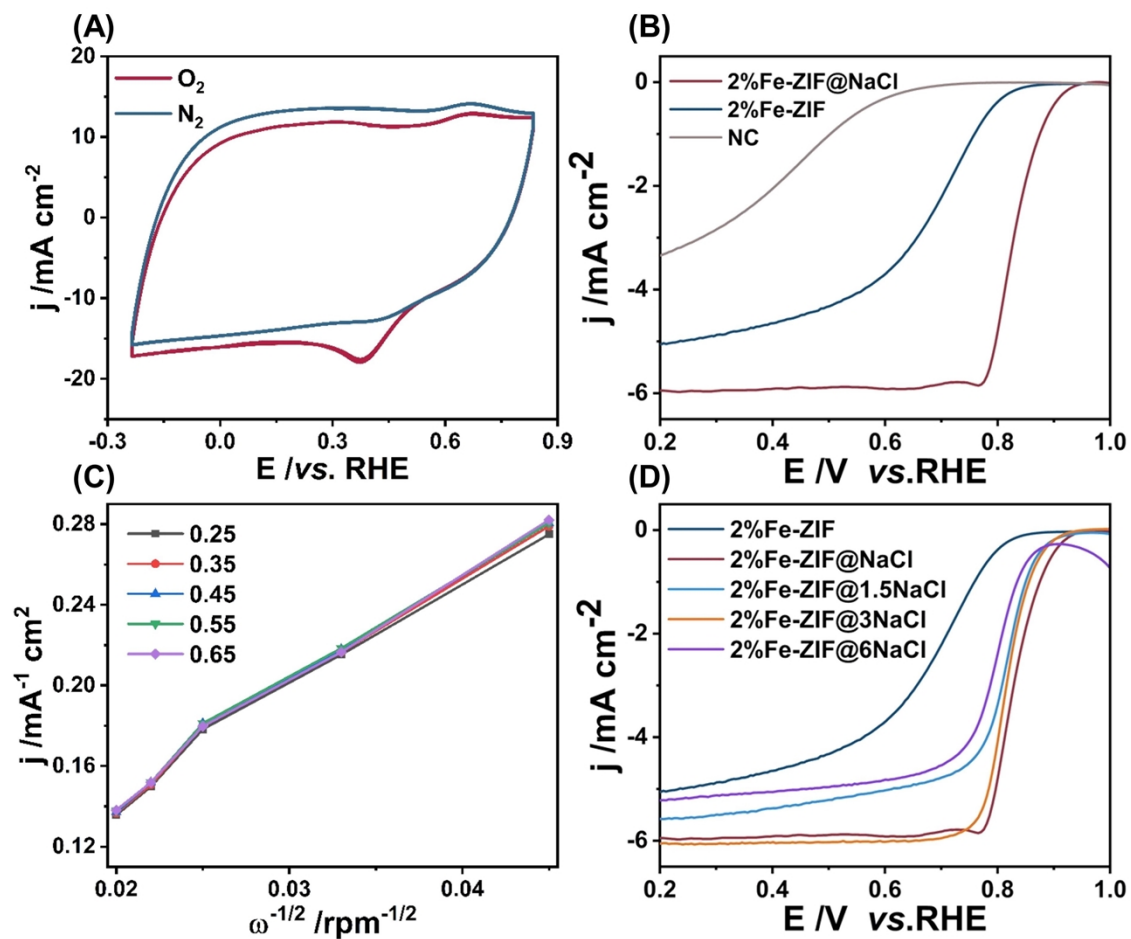
Fig. S8 (A) CV curves of 2%Fe-ZIF-NaCl in N_2 and O_2 saturated in 0.1 M $HClO_4$ electrolyte at 50 mV s^{-1};(B) LSV plots of the catalysts recorded in the O_2 saturated acid electrolyte at 1600 rpm and a scan rate of 10 mV s^{-1};(C) K–L plots of 2%Fe-ZIF@NaCl at different potentials. (D) LSV curves of catalysts with different ratio of NaCl.
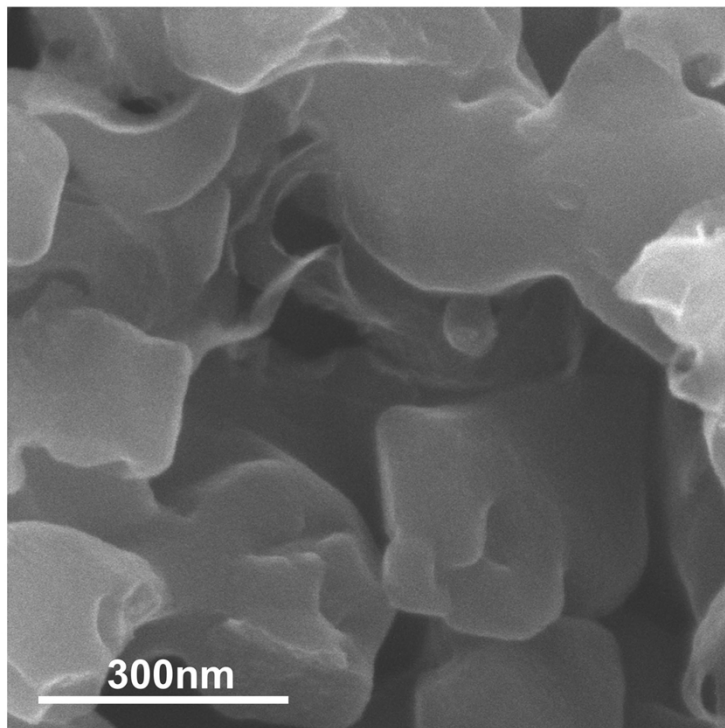
Fig. S9 SEM image of 5%Fe-ZIF@NaCl.

[1]
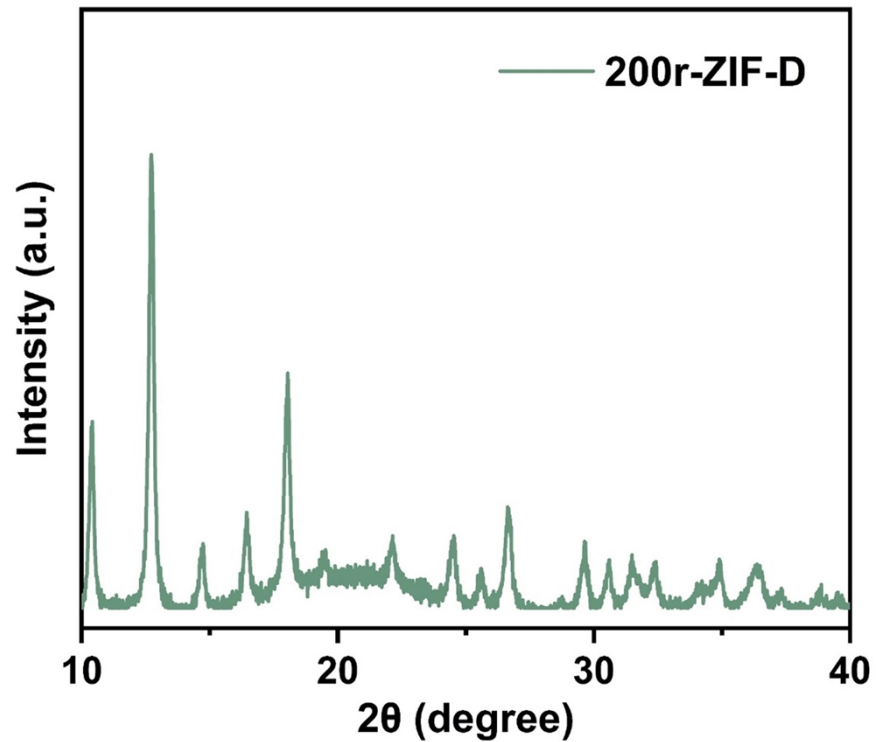
Fig. S10 XRD patterns of ZIF-D.
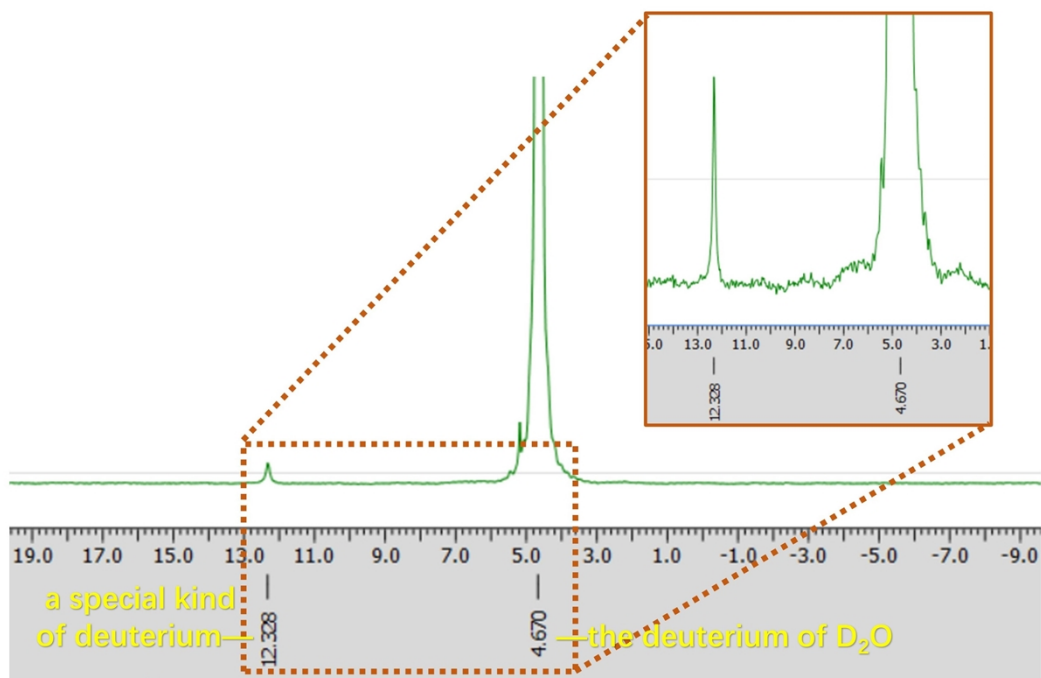
Fig. S11 ^{2}H NMR spectrum of ZIF-D in D_2O.
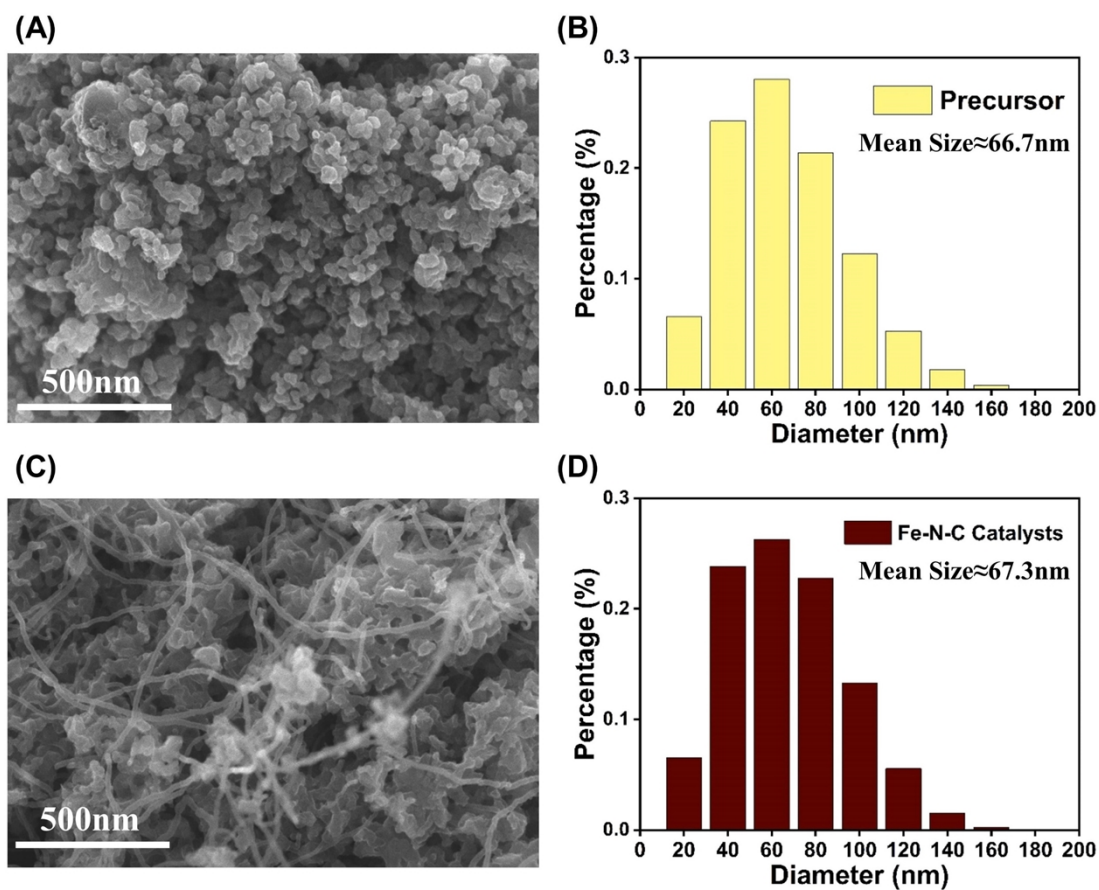
Fig. S12 (A) SEM image;(B) particle size distribution of the ZIF-precursor; (C) SEM image;(D) particle size distribution of the Fe-N-C catalysts.

Table. S1 Pore volume and BET surface areas of 2%Fe-ZIF-NaCl, 2%Fe-ZIF-8 and NC.

	BET surface area (m^2/g)	Pore volume (cm^3/g)
2%Fe-ZIF-NaCl	1444.4	0.930
2%Fe-ZIF-8	974.1	0.830
NC	1052.4	0.997

Table. S2 Elemental quantification determined by XPS for different materials (at. %).

	C	N	O	Zn	Fe
2%Fe-ZIF-NaCl	86.83	6.2	6.3	0.48	0.13
2%Fe-ZIF-8	79.34	7.05	7.82	0.33	0.26

Table. S3 The weight percentage(wt%) of Zn and Fe (determined by ICP-OES) of 2%Fe-ZIF-NaCl and 2%Fe-ZIF-8.

	Zn	Fe
2%Fe-ZIF-NaCl	3.39	1.36
2%Fe-ZIF-8	2.36	1.99

Table. S4 ORR activities of various transition metal singe-atom electrocatalysts synthesized by mechanochemistry strategy.

Catalysts	$E_{1/2}$ (V vs RHE in acidic condition)	Catalyst loading	Date source
2%Fe-ZIF-NaCl	**0.831**	**0.8 mg cm^{-2}**	**This work**
M15-FeNC-NH3	0.782	0.8 mg cm^{-2}	Journal of Energy Chemistry, 2021, 54, 579-586
FeNC-1:20	0.78	0.5 mg cm^{-2}	ACS Appl Mater Interfaces, 2021, 13, 48923-48933
Fe-N-C-10/1-950	0.78	Unclear	ACS Appl Mater Interfaces, 2020, 12,

FeCo/N/C-1:3	0.78	Unclear	17481-17491 Journal of The Electrochemical Society, 2020, 167
B-Zn-FeNG	0.73	0.2038 mg cm^{-2}	J Colloid Interface Sci, 2022, 607, 1201-1214
50-P-Fe/N/G	0.72	0.6 mg cm^{-2}	International Journal of Hydrogen Energy, 2016, 41, 22560-22569
Co-120	0.78	0.8 mg cm^{-2}	Materials Advances, 2022, 3, 1565-1573
Co@NC–MOF–2–900	0.72	0.65 mg cm^{-2}	Small, 2018, 14, e1800441
SOD-Zn0.9Co0.1(CF3-Im)$_2$	0.66	Unclear	Front Chem, 2022, 10, 840758
Mn–N–C–OAc-10-second	0.80	0.8 mg cm^{-2}	Journal of Materials Chemistry A, 2022, 10, 2826-2834

Table. S5 Summary of previously reported Fe-N-C catalysts regarding their ORR

Catalysts	$E_{1/2}$ (V *vs* RHE in acidic condition)	Catalyst loading	Date source
2%Fe-ZIF-NaCl	**0.831**	**0.8 mg cm⁻²**	**This work**
Fe-NC-BU	0.83	0.6 mg cm⁻²	ACS Catalysis, 2022, 12, 6409-6417
FeNC-1:20	0.78	0.5 mg cm⁻²	ACS Appl Mater Interfaces, 2021, 13, 48923-48933
Fe-KJB-3-60a	0.792	0.8 mg cm⁻²	Journal of Materials Chemistry A, 2022, 10, 23001-23007.
Fe-NC $^{\Delta -DCDA}$	0.815	0.2 mg cm⁻²	Nature Catalysis, 2022, 5, 311-323.
1.5Fe-ZIF	0.88	0.8 mg cm⁻²	Energy & Environmental Science, 2019, 12.
Fe/NC-NaCl	0.832	1.2 mg cm⁻²	Advanced Energy Materials, 2021, 11.

activity in acidic condition.

Table. S6 Summary of previously reported Fe-N-C catalysts regarding their ORR activity in H$_2$-O$_2$ MEA conditions.

Catalysts	P_{max} (mW cm^{-2})	Catalyst loading	Date source
2%Fe-ZIF-NaCl	**504.3**	**2 mg cm^{-2}**	**This work**
Fe-NC-BU	700	4 mg cm^{-2}	ACS Catalysis, 2022, 12, 6409-6417
FeNC-1:20	850	4 mg cm^{-2}	ACS Appl Mater Interfaces, 2021, 13, 48923-48933
Fe-KJB-3-60a	348	3 mg cm^{-2}	Journal of Materials Chemistry A, 2022, 10, 23001-23007.
Fe-NC$^{\Delta-DCDA}$	1200	3.9 mg cm^{-2}	Nature Catalysis, 2022, 5, 311-323.
1.5Fe-ZIF	670	4 mg cm^{-2}	Energy & Environmental Science, 2019, 12.
Fe/NC-NaCl	890	4 mg cm^{-2}	Advanced Energy Materials, 2021, 11.

Table. S7 Summary of previously reported Fe-N-C catalysts regarding their ORR activity and mass activity in acidic condition.

Catalysts	$E_{1/2}$ (V vs RHE in acidic condition)	MA on RDE (mA/mg$_{Fe}$@0.9V)	Date source
2%Fe-ZIF-NaCl	**0.831**	**42.6**	**This work**
M15-FeNC-NH3	0.782	27.79	Journal of Energy Chemistry, 2021, 54, 579-586
FeNC-1:20	0.78	28.6	ACS Appl Mater Interfaces, 2021, 13, 48923-48933
Fe-NC-BU	0.83	68.1	ACS Catalysis, 2022, 12, 6409-6417
1.5Fe-ZIF	0.88	136.7	Energy & Environmental Science, 2019, 12.

References

1. X. Xu, X. Zhang, Z. Xia, R. Sun, H. Li, J. Wang, S. Yu, S. Wang and G. Sun, *J. Energy Chem.*, 2021, 54, 579-586.

2. Y. Wu, G. Liang, D. Chen, Z. Li, J. Xu, G. Huang, M. Yang, H. Zhang, J. Chen, F. Xie, Y. Jin, N. Wang, S. Sun and H. Meng, *ACS Appl. Mater. Inter.*, 2021, 13, 48923-48933.

3. Y. Zhan, F. Xie, H. Zhang, Y. Jin, H. Meng, J. Chen and X. Sun, *ACS Appl. Mater. Inter.*, 2020, 12, 17481-17491.

4. G. Liang, J. Huang, J. Li, Y. Wu, G. Huang, Y. Q. Jin, H. Zeng, H. Zhang, J. Chen, Y. Jin, N. Wang, F. Xie and H. Meng, *J. Electrochem. Soc.*, 2020, 167.

5. Y. Liu, J. Bao, Z. Li, L. Zhang, S. Zhang, L. Wang, X. Niu, P. Sun and L. Xu, *J Colloid Inter. Sci.*, 2022, 607, 1201-1214.

6. C. Domínguez, M. A. Peña, S. Rojas and F. J. Pérez-Alonso, *Int. J. Hydrogen Energy*, 2016, 41, 22560-22569.

7. T. Liu, F. Sun, M. Huang and L. Guan, Mater. Adv., 2022, 3, 1565-1573.

8. S. G. Peera, J. Balamurugan, N. H. Kim and J. H. Lee, Small, 2018, 14, e1800441.

9. M. Rautenberg, M. Gernhard, J. Radnik, J. Witt, C. Roth and F. Emmerling, Front. Chem., 2022, 10, 840758.

10. Z. Kong, T. Liu, K. Hou and L. Guan, *J. Mater. Chem. A*, 2022, 10, 2826-2834.

11. J. Zhu, Z. Fang, X. Yang, M. Chen, Z. Chen, F. Qiu, M. Wang, P. Liu, Q. Xu, X. Zhuang and G. Wu, *ACS Catalysis*, 2022, 12, 6409-6417.

12. M. Wang, B. Huang, N. Jiang, T. Liu, J. Huang and L. Guan, Journal of Materials Chemistry A, 2022, 10, 23001-23007.

13. A. Mehmood, M. Gong, F. Jaouen, A. Roy, A. Zitolo, A. Khan, M.-T. Sougrati, M. Primbs, A. M. Bonastre, D. Fongalland, G. Drazic, P. Strasser and A. Kucernak, Nature Catalysis, 2022, 5, 311-323.

14. H. G. Zhang, H. T. Chung, D. A. Cullen, S. Wagner, U. I. Kramm, K. L. More, P. Zelenay and G. Wu, Energy & Environmental Science, 2019, 12.

15. Q. Wang, Y. Yang, F. Sun, G. Chen, J. Wang, L. Peng, W. T. Chen, L. Shang, J. Zhao, D. Sun-Waterhouse, T. Zhang and G. I. N. Waterhouse, Advanced Energy Materials, 2021,